An Empirical Modeling for the Baseline Energy Consumption of an NB-IoT Radio Transceiver

Sikandar M. Zulqarnain Khan, Muhammad Mahtab Alam, *Senior Member, IEEE*, Yannick Le Moullec, *Senior Member, IEEE*, Alar Kuusik, *Member, IEEE*, Sven Pärand, and Christos Verikoukis, *Senior Member, IEEE*

***Abstract*—NarrowBand Internet of Things (NB-IoT) is an emerging cellular IoT technology that offers attractive features for deploying low-power wide-area networks suitable for implementing massive machine-type communications. NB-IoT features include, e.g., extended coverage and deep penetration for massive connectivity, longer battery-life, appropriate throughput, and desired latency at lower bandwidth. Regarding the device energy consumption, NB-IoT is mostly underestimated for its control and signaling overheads, which calls for a better understanding of the energy consumption profiling of an NB-IoT radio transceiver. With this aim, this work presents a thorough investigation of the energy consumption profiling of the radio resource control (RRC) communication protocol between an NB-IoT radio transceiver and a cellular base station. Using two different commercial off the shelf NB-IoT boards and two mobile network operators (MNOs) NB-IoT test networks operational at Tallinn University of Technology, Estonia, we propose an empirical baseline energy consumption model. Based on comprehensive analyses of the profile traces from the widely used BG96 NB-IoT module operating in various states of the RRC protocol, our results indicate that the proposed model accurately depicts the baseline energy consumption of an NB-IoT radio transceiver while operating at different coverage class levels. The evaluation errors of our proposed model vary between 0.33% and 15.38%.**

***Index Terms*—BG96 chip, empirical energy consumption model, LPWAN, narrowband Internet of Things (NB-IoT), NB-IoT networks, power consumption.**

I. Introduction

THE THIRD-GENERATION partnership project (3GPP) has introduced new cellular technologies to enable a wide range of cellular communications specifically for machine-to-machine and Internet-of-Things applications. These include LTE-M (Long-Term Evolution for Machines) and NB-IoT (NarrowBand-IoT) technologies. On one end, LTE-M includes LC-LTE/MTCe (LTE Cat 0) and eMTC (enhanced machine-type communication) technologies (wherein, eMTC includes LTE Cat M1 and LTE Cat M2), particularly targeted at applications that require mobility and higher data rates [1]. On the other hand, NB-IoT includes LTE CAT-NB1 and LTE CAT-NB2 technologies, particularly targeted at applications that require lower complexity and lower data rates [2], [3]. Furthermore, both eMTC and NB-IoT are built upon the existing and already deployed 4G LTE infrastructure to support energy-constrained, mostly battery-powered IoT devices [4].

To reduce the power consumption of an end device, also called a user equipment (UE), both eMTC and NB-IoT provide extended versions of the existing power saving features of the legacy LTE technology, i.e., extended discontinuous reception (eDRX) and power saving mode (PSM), to help prolong the UE's battery lifetime [5], [6]. Utilizing these features in the UE requires a radio resource control (RRC) connection setup between the UE and the network; a detailed overview of this RRC protocol is provided in Section II of this article.

The eDRX feature enables the device to switch off parts of its radio circuitry, thereby operating with limited functionality and, thus, reduced power consumption [7], making it a useful feature for network-oriented applications, where the device can be woken up remotely by the network as needed, e.g., in smart-grid applications. The PSM feature, on the other hand, enables the device to switch off its radio circuity, thereby operating with the lowest possible power consumption [7], making it a useful feature for device-oriented applications, where the device is not accessible to the network but is woken up locally as scheduled (time triggered) by the application, e.g., in smart-metering and public-bike-sharing applications, etc.

A typical NB-IoT device include a radio transceiver, a microcontroller, and additional peripherals as its main components; among them, the radio transceiver has significantly higher energy consumption. Thus, understanding the details of the energy consumption of the radio transceiver is an important research topic in order to better estimate the lifetime of NB-IoT devices.

A. State of the Art

Several works have evaluated the NB-IoT technology in terms of UE's power consumption analysis and battery lifetime estimations [6]–[22]; these works can be categorized into analytical, simulations, and experimental measurement-based

Manuscript received July 29, 2020; revised February 20, 2021; accepted April 2, 2021. Date of publication April 13, 2021; date of current version September 23, 2021. This work was supported in part by the European Union's Horizon 2020 Research and Innovation Program under Grant 668995 and Grant 951867; in part by the European Union Regional Development Fund in the framework of the Tallinn University of Technology Development Program under Grant 2016-2022; and in part by the Estonian Research Council under Grant PRG667. *(Corresponding author: Sikandar M. Zulqarnain Khan.)*

Sikandar M. Zulqarnain Khan, Muhammad Mahtab Alam, Yannick Le Moullec, and Alar Kuusik are with the Thomas Johann Seebeck Department of Electronics, Tallinn University of Technology, 19086 Tallinn, Estonia.

Sven Pärand is with Telia Estonia, 15033 Tallinn, Estonia.

Christos Verikoukis is with the Communication Technologies, Centre Tecnològic de Telecomunicacions de Catalunya, 08860 Castelldefels, Spain.

Digital Object Identifier 10.1109/JIOT.2021.3072769

analyses. Most of these works provide analytical models with simulation-based energy estimations [8]–[16]. For example, the work in [8] focuses on finding the optimum length of an eDRX cycle to help mitigate the signaling cost in an LTE network with simulation-based analysis. Sultania *et al.* [10] have presented an NB-IoT energy consumption model with uplink and downlink data transmissions as defined by the Poisson processes. Tsoukaneri *et al.* [11] and Yeoh *et al.* [12] have tried to estimate the NB-IoT device battery lifetime by using some simplified energy consumption equations, whereas Andres-Maldonado *et al.* [14] have proposed an NB-IoT UE energy consumption analytical model based on the Markov chains. Similarly, the work in [16] presents an analytical model for evaluating the latency and maximum number of devices in any network. Overall, most of the analytical models as presented in these works have been validated through network simulators. Such validations have higher uncertainty as the models' estimates and the validations do not use accurate actual measurements.

Several works have also provided experimental power consumption analysis of the NB-IoT technology, such as [17]–[24]. For example, the work in [17] focuses on the design of an NB-IoT prototype for delay-tolerant applications while operating in different Coverage Levels (CEL) of the network. Although this work provides power consumption measurements of the NB-IoT UE as a whole, the individual power consumption details for each state of the operating mode of radio/node are missing. The work in [18] focuses on the latency issues of NB-IoT while making use of a commercial NB-IoT network in Belgium. Although this work provides empirical results for analyzing the network performance in terms of setup times, throughput, and latency, it does not present the power consumption details of the UE. The work in [19] provides empirical results for the current traces of the CoTS NB-IoT platform, i.e., Ublox SARA-N211 when operating on Vodafone's network in Barcelona, Spain. While this work provides coarse-grained current traces for the various states of the radio, i.e., active waiting (C-DRX mode), Idle waiting (eDRX), and PSM; the underneath fine-grained details for their respective C-DRX cycles, eDRX cycles including paging time windows (PTW) and their underneath I-DRX cycles with sleep periods (SP) and paging occasions (POs) are missing.

Lauridsen *et al.* [21] claim to provide the first publicly available empirical power consumption measurements for the NB-IoT devices but their measurement setup is emulated using a Keysight UXM, a standard-compliant NB-IoT BS emulator. That is why it is unclear as to what extent their results would map onto a real network. Similarly, the work in [23] proposes a Dual-RAT LPWAN node combining an NB-IoT and LoRaWAN radio into one node with all the necessary power regulator circuitry. Here too, the power consumption numbers are given for the whole node only, and the individual power graphs for the radio modes and their internal state details are missing.

Considering the above sate-of-the-art and to the best of our knowledge, the following research gaps exist in the literature. First, no detailed baseline power consumption assessment of the NB-IoT radio has yet been provided. Second, an accurate energy consumption model that truly depicts the empirical energy consumption of an NB-IoT radio across its various stages of RRC operation (i.e., attach, active waiting, idle waiting, and resume) is missing. Third, recently published works on the NB-IoT UE's power consumption present only a coarse-grain analysis of the NB-IoT node(s), mostly providing the aggregated power consumption of the whole node, where the individual power consumption details of the underneath activities remain mostly obscured. In other words, the detailed energy-consumption profiling of the various states of the CoTS NB-IoT radio module(s) and its underneath activities remain unexplored to date. Fourth, most of the existing analyses are based on emulated NB-IoT networks [in particular, the base-station (BS)] and not on actual network operating BS. Similarly, the detailed energy consumption profiling of the commercially available (CoTS) NB-IoT devices under real mobile network operators (MNOs) networks are yet to be explored.

B. Contributions

This work provides a modeling methodology for profiling the baseline energy consumption of an NB-IoT radio transceiver based on detailed empirical measurements. The modeling methodology considers all the states of the RRC protocol standardized by 3GPP and, hence, is applicable to general NB-IoT radio chips that are standard compliant.

The main contributions of our article and its positioning with reference to the state of the art can be summarized as follows.

1) Decomposition of the LTE RRC protocol with precise details and experimental demonstrations: while the 3GPP standard documentation ([6], [25]–[27]) and a number of papers in the literature (among others [19]) present the key concepts of the LTE RRC protocol, to the best of our knowledge, this work is the first one to delve into a fine-grained analysis of the LTE RRC protocol while mapping its different stages and modes with equally detailed experimental results in terms of energy consumption, thereby providing details and an understanding of the baseline energy consumption at a level not available so far.
2) Empirical and detailed power consumption measurements of CoTS NB-IoT radio transceiver while operating under real networks: in contrast to most existing works (e.g., [19], [21], and [23]) that are limited to the aggregated power or energy consumption of the whole NB-IOT UE and/or rely on either simulations or emulated networks, this work analyzes the energy consumption of the radio transceiver in detail (i.e., for each state of the RRC protocol) while operating under two MNOs-deployed NB-IoT test networks; this provides not only a more detailed analysis but also more realistic, empirical-based results as compared to the state of the art.
3) The derivation of an accurate energy consumption model for an NB-IoT radio transceiver: existing models are

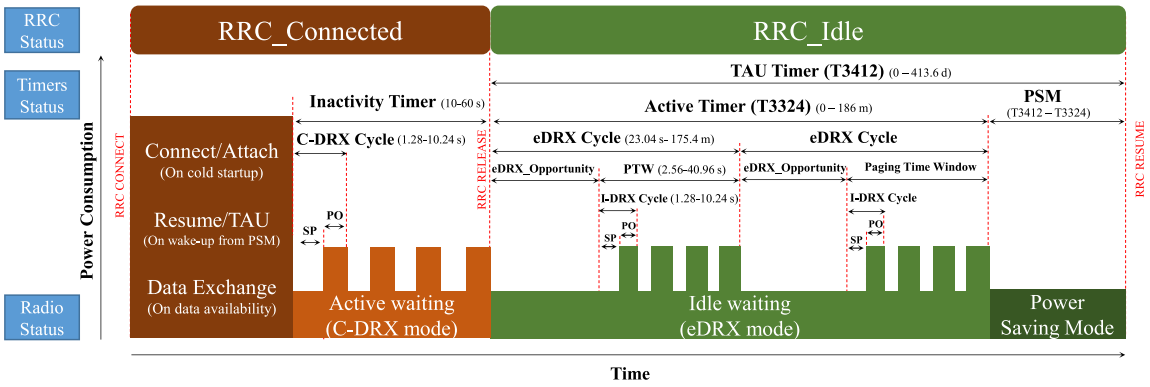

Fig. 1. RRC protocol reference model for the NB-IoT radio. It is composed of two complementary states, i.e., RRC_Connected and RRC_Idle and exploits Active waiting, Idle waiting, and Power Saving Mode (PSM) after establishing a connection with the network. From top to bottom: (top) RRC connection status, (middle) timers with their minimum and maximum limits, and (bottom) radio status with associated power consumption, as depicted schematically.

analytical only and/or not detailed enough to reflect all the inner mechanisms at play in the NB-IoT radio. To overcome this gap, and to the best of our knowledge, this article is the first one to propose a detailed and realistic NB-IoT radio transceiver energy consumption model, thanks to the detailed analysis and real-life empirical experiments mentioned above.

4) The proposed model is evaluated under real life conditions and we calculate the difference between the energy consumption obtained from the real-life deployment versus the energy consumption predicted by using our proposed model. Our results show that the error of the proposed model ranges between 0.33% and 15.38%, with the largest deviations occurring in the attach and resume procedures.

The remainder of this article is organized as follows. Section II provides an overview of the RRC protocol, whereas Section III presents our proposed NB-IoT radio energy consumption model. Section IV presents the empirical measurement results of the NB-IoT radio energy consumption at its various states of operation and Section V presents the evaluation of the proposed model. Section VI summarizes our conclusions and future works.

II. Overview of Radio Resource Control (RRC) Protocol

The RRC is a communication protocol between an end device/UE and the BS [also termed evolved Node-B (eNB)] through which network services, such as connection establishment, connection maintenance, data exchange, sleep and notification patterns, security and Quality of Service (QoS), etc., take place. The RRC protocol model has only two complementary states , i.e., 1) RRC_Connected and 2) RRC_Idle, as shown in the RRC protocol reference model in Fig. 1; the radio alternates between these two states during operation.

As shown in Fig. 1, the UE, on power up (or cold start), requests a network connection from the BS which upon acknowledgement is granted network resources and it thus enters into the RRC_Connected state. The connection establishment takes place in the "Attach" procedure and is always initiated by the UE. Once connected, the exchange of [uplink(Tx)/downlink(Rx)] data between the UE and the network takes place in the allocated transmission and reception slots that have been previously allocated to the UE during the "Attach" procedure. After a secure exchange of data, the UE listens to the broadcast information from the eNB for a certain period of time that is termed as "Active waiting" and whose period is set by the network operator. If any data arrive during this period, the RRC connection is resumed for the exchange of data between the UE and the network such that active waiting period restarts at the end of the data exchange. However, if no data arrive during active waiting, the eNB releases the connection and the UE switches to the RRC_Idle state, thereby saving all the context of the network in local memory.

Transiting into RRC_Idle state, the UE may enter either into eDRX or into PSM as per its configuration. The UE can also alternate between these two states, with eDRX first and PSM next, incase if both states are enabled. In the eDRX mode, the UE listens to the broadcast information from the eNB in cyclic patterns known as eDRX cycles; hence, this phase is termed the eDRX mode. When the eDRX mode expires or when it is forced to expire, the UE switches to the PSM mode during which it turns off its radio and is, therefore, not reachable by the network. This mechanism facilitates the device to enter deeper hardware sleep modes and thus contribute toward maximum power savings of the UE's battery, but at the cost of increased latency.

To summarize, the NB-IoT radio goes through the following states as it operates under the RRC protocol , i.e., 1) *Attach*—Registration to the network on a cold start or power up; 2) *Data Exchange (Tx/Rx)*—transmission and reception of data to/from the network; 3) *Active Waiting (C-DRX Mode)*—continuous listen to the broadcast information from the eNB for a period as permitted by the network operator and as configured by the UE; 4) *Idle Waiting (eDRX mode)*—partly listens to the broadcast information from eNB for a period as permitted by the operator and as configured by the UE; 5) *Power Saving Mode (PSM)*—shutdown of the radio activity for a period as requested by the UE and that as acknowledged by the network; and 6) *Tracking Area Update (TAU)*—resuming the connection with eNB on wake up from PSM.

All these radio states are shown in the RRC reference model in Fig. 1.

Details of these radio states are discussed in what follows.

A. Attach—RRC_Connected State

On powering up, the radio scans the air for a suitable network interface through a contention-based random access (RA) preamble to which the eNB responds with a random access response (RAR) message. The UE then sends an RRC connection request to which the eNB responds with an RRC connection setup and the UE thus gets connected to the eNB. Afterward, the UE establishes a connection with the core network and generates an access stratum (AS) security context for secure exchange of data. After a successful AS security setup, the eNB reconfigures the RRC connection to finally establish a data radio bearer for the UE to uplink its data packets in the allocated transmission (Tx) slots. Further details on the attach procedure can be found in [26] and [27].

B. Data Exchange (Tx/Rx)—RRC_Connected State

When the UE wants to transmit some data to the network, it first establishes an RRC connection with the network through an Attach procedure (on powering up) or TAU procedure (on waking up from PSM) and transits to the RRC Connected state. It then transmits its data packets to the network in its allocated transmission (Tx) slots using some transmission protocols (such as UDP, HTTPS, MQTT, etc). On the other hand, when the network wants to transmit some data to the UE (i.e., the UE will now receive data), there are two possibilities for the network to reach the UE in its RRC_Idle state, depending on whether it is in eDRX or PSM mode. If the UE is in eDRX mode, it periodically listens to the broadcast messages from the network during the paging occasion (PO) of each I-DRX cycle. In this case, the network sends a paging message to the UE and notifies it of the pending downlink traffic. As the UE interprets the paging message, it initiates a connection resume/reconnect procedure to get connected to the network and, thus, the exchange of downlink data between the UE and network occurs in the allocated reception (Rx) slots. However, if the UE is in PSM mode, it is not reachable by the network until the expiration of its PSM period (i.e., T3412-T3324). As the PSM expires, the UE initiates the TAU procedure to resume connection with the network, after which the data exchange occur. More details on data exchange can be found in [13] and [28].

C. Active Waiting—RRC_Connected State

Discontinuous reception (DRX) is a legacy LTE feature that enables the UE to discontinuously receive the physical downlink control channel (PDCCH) to maintain network synchronization and determine if there is any pending downlink data. In the LTE RRC protocol, the DRX feature can be enabled both in the RRC_Connected state, i.e., Connected-DRX (C-DRX), and in the RRC_Idle state, i.e., Idle-DRX (I-DRX). In the RRC_Connected state, when there is no data traffic, the UE alternates between a sleep period (SP) during which the radio remains quiet and a paging occasion (PO), also called the paging event (PE), during which the radio monitors the PDCCH such that SP and PO alternates in a cyclic pattern that is termed the C-DRX cycle (where *C* stands for the connected state of the radio). These SPs and POs patterns (i.e., C-DRX cycles) repeat for the entire duration of "Active waiting" phase and whose length is controlled by the value of the inactivity timer. The value of the inactivity timer is operator specific (10–60 s in most commercial networks) and the UE cannot override its value as set by the operator. Furthermore, the inactivity timer starts running automatically; either at the end of data exchange between the UE and the network or when no data are available after the Attach procedure, where upon its expiration, the network releases the connection and the device switches to RRC_Idle state [25]. If some data arrive while the UE is still active waiting (i.e., Inactivity Timer is running), the connection is resumed for the exchange of data between the UE and the network; the inactivity timer restarts at the end of this data exchange and the UE enters into its active waiting phase again.

D. Idle Waiting (eDRX Mode)—RRC_Idle State

In the RRC_Idle state, new resources cannot be requested from the network. However, the UE is still reachable by the network, where it periodically monitors the physical downlink control channel (PDCCH) in cyclic patterns. The NPDCCH monitoring takes place during the on-phase of an I-DRX cycle (where I stands for Idle state of the radio), i.e., PO or PE, whereas during the next off-phase of the I-DRX cycle, i.e., SP, the radio does not perform any activity. These I-DRX cycles repeat for the entire duration of a paging time window (PTW). A PTW itself forms the active phase of an eDRX Cycle such that each PTW is followed by an inactive phase that is termed an eDRX_Opportunity and during which the radio remains inoperative for until the beginning of the next PTW. These cyclic patterns of eDRX_Opportunity and PTW, i.e., eDRX Cycles occur repeatedly during the entire span of the idle waiting state of the radio. Since idle waiting involves repeated eDRX cycles, this phase is also termed the eDRX mode. All these nested cycles of activity and inactivity periods occurring during the eDRX mode are shown in the RRC protocol reference model in Fig. 1.

The eDRX mode is controlled by a set of timers where the active timer (i.e., T3324) primarily controls the time lapse of the entire duration of the eDRX mode and can have an extended range from 0 to 186 min for NB-IoT, with a maximum period of 175.4 min for its eDRX cycle and a maximum period of 40.96 s for its PTW. The maximum I-DRX cycle can be of 10.24 s for NB-IoT. The minimum and maximum limits of these cycles for NB-IoT technology are also indicated in the RRC protocol reference model in Fig. 1. Further details on their minimum and maximum ranges can be found in [6] and [7]. It is worth mentioning here that the UE can configure the length of its eDRX mode, the length of its eDRX cycle, and the duration of its PTW, only if permitted by the network.

E. PSM—RRC_Idle State

On expiration of the active (T3324) timer, the UE exits idle waiting (eDRX mode) and enters into a power saving mode (PSM). While in PSM, the UE turns its radio off for as

long as the TAU timer is running and its energy consumption approaches to almost that of its power-off state. It is worth noting that though the radio or UE is not reachable by the network, it is still registered with the network, so that when the UE wakes up from PSM, it does not have to go through the registration process all over again; this adds to a significant amount of energy savings in reducing the signaling overhead. Further details on the resume procedure can be found in [15], [26], [27], and [28].

As the TAU (T3412) timer expires, the PSM is exited and the UE wakes up to perform the "Tracking Area Update (TAU)" procedure when the already registered UE reconnects with the network to check for any pending uplink/downlink data. Once this data exchange has occurred, the active waiting period restarts; when it ends, the UE enters into the RRC_Idle state and the cycle repeats. It should be noted here that the PSM mechanism implies a low power consumption at the cost of higher latency. Because the network has to wait until the UE is up again from its PSM and reachable by the network. As NB-IoT is designed for latency-tolerant applications, the UE may (deep) sleep for an extended range of up to 413 days and still be registered with the network. More details on the PSM state can be found in [6] and [19].

F. Tracking Area Update (TAU)—RRC_Connected State

On expiration of the TAU (T3412) timer, the device wakes up from its PSM and reconnects to the network to indicate its availability in the TAU procedure. During the TAU procedure, the UE listens to any scheduled DL data that, if exist, are downloaded in the allocated reception (Rx) slots. Similarly, if the UE has any UL data, it is transferred to the network in the allocated transmission (Tx) slots. If no data exist for exchange, the inactivity timer starts so that the device enters into the active waiting phase. As it finishes, the device enters into idle waiting and the cycle continues. Further details on the TAU procedure can be found in [6], [26], and [27].

This section has presented an in-depth analysis of the NB-IoT RRC protocol phases; thanks to this knowledge, we can now proceed with building an empirical NB-IoT UE energy consumption model, which we describe in the next sections.

III. Proposed Model for Profiling the Baseline Energy Consumption of NB-IoT Radio Transceiver

In addition to the detailed analysis of the RRC protocol presented in the previous section, an empirical model that provides a detailed baseline energy consumption of the RRC protocol is presented in this section.

Since the RRC protocol has only two states, i.e., 1) RRC_Connected and 2) RRC_Idle, the total energy consumed by an RRC radio can be given as

$$E_{\text{TOTAL}} = E_{\text{RRC\_CONNECTED}} + E_{\text{RRC\_IDLE}}. \tag{1}$$

In the RRC_Connected state, the radio goes through the four following states, i.e., Attach, Data Exchange (Tx/Rx), Active waiting (C-DRX), and TAU. The Attach procedure occurs only after a cold start; whereas, the TAU procedure occurs each time the radio wakes up from PSM. Thus, the total energy consumed during the RRC_Connected state can be written as

$$E_{\text{RRC\_CONNECTED}} = E_{\text{ATTACH}} + E_{\text{Tx/Rx}} + E_{\text{C-DRX}} + E_{\text{TAU}}. \tag{2}$$

As the inactivity timer finishes, the RRC connection is released and the radio goes into the RRC_Idle state where the radio first enters into Idle waiting state or eDRX mode, followed by PSM. Thus, the total energy consumed during the RRC_Idle state can be written as

$$E_{\text{RRC\_IDLE}} = E_{\text{eDRX}} + E_{\text{PSM}}. \tag{3}$$

Since Energy = Power × Time, the average energy consumption during the RRC_Connected state can be written as

$$\begin{aligned} E_{\text{RRC\_CONNECTED}} = {} & \left\{P_{\text{ATTACH(avg)}} \times T_{\text{ATTACH}}\right\} \\ & + \left\{\left(P_{\text{Tx(avg)}} \times T_{\text{Tx}}\right) + \left(P_{\text{Rx(avg)}} \times T_{\text{Rx}}\right)\right\} \\ & + \left\{P_{\text{C-DRX(avg)}} \times T_{\text{InactivityTimer}}\right\} \\ & + \left\{\text{P}_{\text{TAU(avg)}} \times \text{T}_{\text{TAU}}\right\}. \end{aligned} \tag{4}$$

Since the ActiveWaiting (C-DRX mode) period is a series of repeated C-DRX cycles, the above equation can be rewritten as

$$\begin{aligned} E_{\text{RRC\_CONNECTED}} = {} & \left\{P_{\text{ATTACH(avg)}} \times T_{\text{ATTACH}}\right\} \\ & + \left\{\left(P_{Tx\text{(avg)}} \times T_{\text{Tx}}\right) + \left(P_{Rx\text{(avg)}} \times T_{\text{Rx}}\right)\right\} \\ & + \left\{P_{\text{C-DRX(avg)}} \times \left(T_{\text{CDRX\_Cycle}} \times N_{\text{CDRX\_Cycles}}\right)\right\} \\ & + \left\{P_{\text{TAU(avg)}} \times T_{\text{TAU}}\right\} \end{aligned} \tag{5}$$

where $T_{\text{CDRX\_Cycle}}$ is the time period of each C-DRX cycle, and $N_{\text{CDRX\_Cycle}}$ is the total number of C-DRX cycles that occur during the ActiveWaiting period.

Similarly, the average energy consumption of the radio during the RRC_Idle state is

$$E_{\text{RRC\_IDLE}} = E_{\text{eDRX}} + E_{\text{PSM}} \tag{6}$$

and can be rewritten as

$$E_{\text{RRC\_IDLE}} = \left\{P_{\text{eDRX(avg)}} \times T_{\text{eDRX}}\right\} + \left\{(P_{\text{PSM(avg)}} \times T_{\text{PSM}}\right\}. \tag{7}$$

The duration of the entire Idle state of the radio, and its eDRX and PSM durations, can be set by the values of 3GPP-specified timers, such that

$$T_{\text{RRC\_IDLE}} = T_{3412} \tag{8}$$

$$T_{\text{eDRX}} = T_{3324} \tag{9}$$

$$T_{\text{PSM}} = T_{3412} - T_{3324}. \tag{10}$$

Thus, the average energy consumption of the radio during the RRC_Idle state can be rewritten as

$$\begin{aligned} E_{\text{RRC\_IDLE}} = {} & \left\{P_{\text{eDRX(avg)}} \times T_{3324}\right\} \\ & + \left\{P_{\text{PSM(avg)}} \times (T_{3412} - T_{3324})\right\}. \end{aligned} \tag{11}$$

Since, the eDRX mode is composed of repeated eDRX cycles, thus

$$E_{\text{RRC\_IDLE}} = \left\{P_{\text{eDRX(avg)}} \times \left(T_{\text{eDRX\_Cycle}} \times N_{\text{eDRX\_Cycles}}\right)\right\} + \left\{\left(P_{\text{PSM(avg)}} \times (T_{3412} - T_{3324})\right\}\right. \quad (12)$$

where $T_{\text{eDRX\_Cycle}}$ is the time period of each eDRX cycle and $N_{\text{eDRX\_Cycles}}$ is the total number of eDRX cycles that occur during the IdleWaiting period.

Since each eDRX cycle is composed of a PTW (active phase of an eDRX cycle) and eDRX_opportunity (inactive phase of an eDRX cycle), the above equation can be expanded to

$$E_{\text{RRC\_IDLE}} = \left\{P_{\text{eDRX(avg)}} \times \left(T_{\text{eDRX\_PTW}} + sT_{\text{eDRX\_OPP}}\right) \times N_{\text{eDRX\_Cycles}}\right\} + \left\{\left(P_{\text{PSM(avg)}} \times (T_{3412} - T_{3324})\right\}\right. . \quad (13)$$

Moreover, since the power consumption of PTW and eDRX_opportunity during each eDRXcycle is different, the above equation can be written as

$$E_{\text{RRC\_IDLE}} = \left\{\left(P_{\text{eDRX\_PTW(avg)}} \times T_{\text{eDRX\_PTW}}\right) + \left(P_{\text{eDRX\_OPP(avg)}} \times T_{\text{eDRX\_OPP}}\right) \times N_{\text{eDRX\_Cycles}}\right\} + \left\{\left(P_{\text{PSM(avg)}} \times (T_{3412} - T_{3324})\right\}\right. . \quad (14)$$

As PTW is a repeated sequence of I-DRX cycles, the above becomes

$$E_{\text{RRC\_IDLE}} = \left\{\left(P_{\text{eDRX\_PTW(avg)}} \times \left(T_{\text{I-DRX\_Cycle}} \times N_{\text{I-DRX\_Cycles}}\right) + \left(P_{\text{eDRX\_OPP(avg)}} \times T_{\text{eDRX\_OPP}}\right) \times N_{\text{eDRX\_Cycles}}\right\} + \left\{\left(P_{\text{PSM(avg)}} \times (T_{3412} - T_{3324})\right\}\right. \quad (15)$$

where $T_{\text{I-DRX\_Cycle}}$ is the time period of each $\text{I}-\text{DRX}$ cycle and $N_{\text{I-DRX\_Cycles}}$ is the total number of $\text{I}-\text{DRX}$ cycles occurring during the PTW of each eDRXcycle.

Next, since each $\text{I}-\text{DRX}$ cycle has an on phase (i.e., PO) during which the NPDSCCH signal is monitored and an off phase with no activity, the above equation can be expanded to

$$E_{\text{RRC\_IDLE}} = \left\{\left(P_{\text{I-DRX\_on(avg)}} \times T_{\text{I-DRX\_on}}\right) + \left(P_{\text{I-DRX\_off(avg)}} \times T_{\text{I-DRX\_off}}\right) \times N_{\text{I-DRX\_Cycles}}) + \left(P_{\text{eDRX\_OPP(avg)}} \times T_{\text{eDRX\_OPP}}\right) \times N_{\text{eDRX\_Cycles}}\right\} + \left\{\left(P_{\text{PSM(avg)}} \times (T_{3412} - T_{3324})\right\}\right. . \quad (16)$$

Finally, given that

$$E_{\text{TOTAL}} = E_{\text{RRC\_CONNECTED}} + E_{\text{RRC\_RELEASED}} \quad (17)$$

we obtain

$$E_{\text{TOTAL}} = \left\{\left\{P_{\text{ATTACH(avg)}} \times T_{\text{ATTACH}}\right\} + \left\{\left(P_{\text{Tx(avg)}} \times T_{Tx}\right) + \left(P_{\text{Rx(avg)}} \times T_{Rx}\right)\right\} + \left\{P_{\text{C-DRX(avg)}} \times \left(T_{\text{CDRX\_Cycle}} \times N_{\text{CDRX\_Cycles}}\right)\right\} + \left\{P_{\text{TAU(avg)}} \times T_{\text{TAU}}\right\}\right\} + \left\{\left\{\left\{\left(P_{\text{I-DRX}_{\text{on(avg)}}} \times T_{\text{I-DRX}_{\text{on}}}\right) + \left(P_{\text{I-DRX}_{\text{off(avg)}}} \times T_{\text{I-DRX}_{\text{off}}}\right) \times N_{\text{I-DRX\_Cycles}}\right\} + \left\{\left(P_{\text{eDRX\_OPP(avg)}} \times T_{\text{eDRX\_OPP)}}\right\} \times N_{\text{eDRX\_Cycles}}\right\} + \left\{P_{\text{PSM(avg)}} \times (T_{3412} - T_{3324})\right\}\right\}. \quad (18)$$

For simplicity, the above equation can be rearranged in terms of the 3GPP-specified timers such that each row in the following equation represents the energy consumption of each separate state of the radio, i.e., Attach, Data Exchange [Transmit (Tx) and Receive (Rx)] , Active waiting (C-DRX mode), Idle waiting (eDRX mode), deep sleep mode (PSM) and Resume (TAU), i.e.,

$$E_{\text{TOTAL}} = \begin{pmatrix} \left\{P_{\text{ATTACH(avg)}} \times T_{ATTACH}\right\} \\ +\left\{\left(P_{\text{Tx(avg)}} \times T_{\text{Tx}}\right) + \left(P_{\text{Rx(avg)}} \times T_{\text{Rx}}\right)\right\} \\ +\left\{P_{\text{C-DRX(avg)}} \times (T_{\text{InactivityTimer}})\right\} \\ +\left\{P_{\text{TAU(avg)}} \times T_{\text{TAU}}\right\} \end{pmatrix} + \begin{pmatrix} \left\{\left(P_{\text{eDRX(avg)}} \times T_{3324)}\right\} \\ +\left\{P_{\text{PSM(avg)}} \times (T_{3412} - T_{3324})\right\}. \end{pmatrix} \quad (19)$$

This section has presented the proposed NB-IoT UE energy consumption model. The next sections detail the corresponding results and corresponding evaluations.

IV. Empirical Measurements

As explained in Section I-A, works on experimental energy consumption profiling of NB-IoT radio transceivers are limited. To overcome the limitations of the state of the art, a comprehensive model for profiling the empirical energy consumption of an NB-IoT radio transceiver using the RRC protocol has been proposed in the previous section. The proposed model relies on empirical measurements; this section presents our experimental setup and measurement results obtained with two widely used CoTS NB-IoT radio boards (both equipped with BG96 module) with network configurations from two MNOs (referred to as Operator 1 and Operator 2) operating NB-IoT test networks at Tallinn University of Technology.

A. Experimental Setup

The two CoTS NB-IoT radio modules, i.e., Avnet Silica NB-IoT sensor shield [29] and Quectel UMTS & LTE EVB Kit [30], are based on the 3GPP Rel-13 compliant Quectel BG96 LPWAN module [31]. They are used for conducting the current and power consumption measurements, while in actual operation, under the two publicly available test networks provided by Operator 1 and Operator 2.

A Keysight Technologies N6705C DC Power Analyzer (PA) [32] is used for collecting the current and power traces during these measurement campaigns. Our test-bed setup, composed of an Avnet shield as our device under test (DUT) DUT1 and Quectel EVB Kit as our DUT2, along with the Keysight's PA, is shown in Fig. 2. A constant voltage of 3.3 V is supplied to DUT1 and 3.8 V to DUT2 by the PA. AT commands are sent from the QCOM software running on the PC through the USB-PMOD interface for DUT1 and through the USB interface, configured accordingly, for DUT2. SIM cards for both the

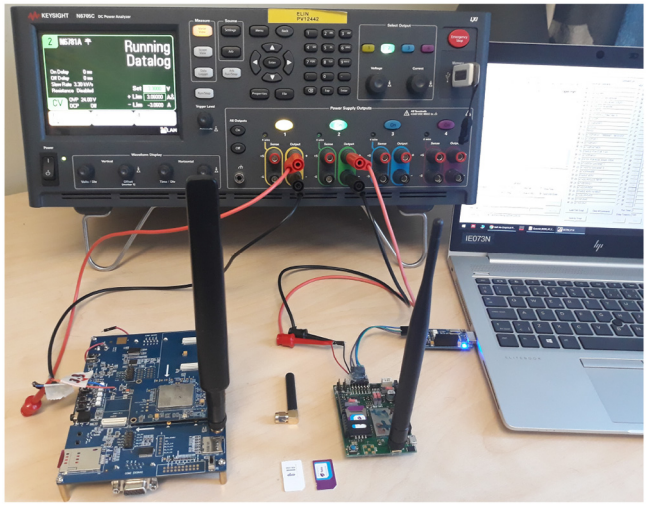

Fig. 2. Testbed Setup with Quectel BG96 and Avnet Silica BG96 NB-IoT radio modules, Keysight N6705C DC Power Analyzer, and SIM cards from Operator 1 and Operator 2.

TABLE I
DETAILS OF THE PUBLICLY AVAILABLE NB-IOT NETWORKS THAT HAVE BEEN USED DURING OUR MEASUREMENT CAMPAIGNS ON TEST LOCATION

Details	Operator 1	Operator 2
Operator numeric code	24801	24802
Selected Access Technology	CAT-NB1	CAT-NB1
Selected Band	LTE BAND 20	LTE BAND 20
Selected Channel ID	6254	6152
CE level (at test locations)	0 , 1	0 , 1
SNR {0(bad) to 31(good)}(dB)	28 , 6 (avg)	21 , 5 (avg)
SINR{0(bad) to 250 (good)}(dB)	185, 178 (avg)	153, 142 (avg)
RSSI{-110(bad) to -60(good)}(dBm)	-67, -101 (avg)	-72, -110 (avg)
RSRP{-140(bad) to -44(good)}(dBm)	-67, -111 (avg)	-74, -117 (avg)
RSRQ{-19.5(bad) to -3(good)}(dB)	-3 , -9 (avg)	-3 , -10 (avg)

networks under test are also visible in our setup, as shown in Fig. 2.

From a practical perspective, it should be mentioned that though the BG96 module of both DUTs were flashed with the latest firmware (FW) version, setting up the (T3324/T3412) timers to our desired values was a cumbersome procedure. Upon contacting Quectel, it turned out that even the latest FW (i.e., BG96MAR02A07M1G) has updates in the form of subversions; installing the latest subversion (i.e., BG96MAR02A07M1G_01.016.01.016) solved most of the Timers' related issues. Similarly, the built-in USB-USB interface on DUT1 that is provided to receive power and AT commands from a PC disrupted the power measurements from the PA. To avoid these disruptions, we used an FTDI chip-based serial communication interface to utilize its built-in USB-UART PMOD interface [33] and bypassed its USB-USB port. We also disabled all the functional LEDs [34] of DUT1 to get accurate power consumption measurements from the PA. As for testing DUT2, we also modified it as per the documents provided to us by the Quectel Team. Finally, the details of the two MNOs NB-IoT test networks that have been considered for carrying out this research are summarized in Table I.

During our measurement campaign, the NB-IoT devices were placed at different locations inside Thomas Johann Seebeck Department of Electronics building and students' dormitory building that are located on TalTech campus. For triggering the different CEL, the devices were deployed on the second basement (B2) floor of Thomas Johann Seebeck Department of Electronics building, where the received signal strength is lower than on the upper floors. On each test location, the current value of the CE level was queried using the adequate AT commands and when the required CE levels were achieved, i.e., CE Level 0 and CE Level 1, the measurements were made accordingly.

TABLE II
OPERATOR SPECIFIC AND UE CONFIGURABLE PARAMETERS

Network Params	Symbol	Value
Attach	*T_ATTACH*	Network_conditions
Inactivity Timer	*InactivityTimer*	Operator_defined
C-DRX Cycle	*CDRX_Cycle*	Operator_defined
RRC_Idle	*RRC_Idle*	UE defined = T3412 Timer value
Active Timer	*T3324 Timer*	UE defined = T3324 Timer value
eDRX Cycle	*eDRX_Cycle*	Network defined; UE configurable
PagingTimeWindow	*PTW*	Network defined; UE configurable
eDRX_Opportuity	*eDRX_Opp*	(eDRX_Cycle - PTW)
I-DRX Cycle	*I-DRX_Cyc*	Operator_defined
PowerSavingMode	*PSM*	UE defined = (T3412-T3324) value

Small differences between the two operators in terms of their SNR, SINR, RSSI, RSRP, and RSRQ for the same CE levels could be observed from their respective values as given in Table I. However, to smooth out the minor variations of the individual results for SNR, SINR, RSSI, RSRP, and RSRQ; their experiments were repeated in the order of 100 times on each test location and the obtained results were averaged into their final values, under their respective CE levels, as summarized in Table I. Table II summarizes the network parameters that are operator specific and/or UE configurable with a short description of their control and possible values.

B. Measurements Approach

The Data Logger function of the Keysight PA records the output (voltage, current, and power) data logs of the arbitrary waveform at a sampling rate of 50 kHz. The display of the PA can be configured to examine these waveforms with a precision of up to 20 μs. For example, in Fig. 3, the waveform of the power consumption of BG96 radio under real network is recorded as a data log file from the Keysight PA. This data log file is displayed in the "Maker View" of the data logger screen where the power trace P1 (Label 3 in Fig. 3) is displayed with 100 mW/Div (Label 1 in Fig. 3) on vertical/power scale and 20.0 s/d (Label 4 in Fig. 3) on the horizontal/time scale of the PA screen. The voltage (V1) and current (I1) (under Label 1 in Fig. 3) are not selected for readability. The markers m1 and m2 (Label 2 in Fig. 3) are set to positions, where they intersect the P1 trace of the BG96 radio at the beginning and end of its C-DRX mode (Active waiting); thus, the information available under Labels 5 to 10 presents the data available between m1 and m2 markers and can be read as summarized in Table III.

All the measurement results presented in rest of this article are recorded as data log files and displayed in the Marker view of the PA, similar to the one as shown in Fig. 3. This approach is used to produce actual power traces of the BG96 radio under

TABLE III
READING DATA FROM THE MARKER VIEW OF THE POWER ANALYZER

Symbol/Field	Description
1 Trace Controls	Identifies the voltage/div. or current/div. settings. Tick ($\surd$) indicates the trace is on. Dots ($\cdots$) indicate the trace is off. *In current setup, we only select the power trace.*
2 m1/m2 markers	Shows where the measurement markers intersect the selected waveform. Data values at the bottom of the display (i.e. labelled 5-10) are referenced to the intersect locations of the markers. Calculations are based on the data points in between the intersect locations.
3 Data Trace	Voltage, Current, Power trace as selected in Label 1.
4 Time/Div.	Identifies the horizontal time-base setting , i.e. the scale of each horizontal square on the screen.
5 m1	Indicates the m1 marker value in volts, amps, or watts at the intersection point. Also indicates the distance in time of the m1 marker in relation to the present trigger position.
6 m2	Indicates the m2 marker value in volts, amps, or watts at the intersection point. Also indicates the distance in time that the m2 marker is in relation to the present trigger position.
7 Delta	Indicates the absolute difference (Δ) between the markers in units (volts, amps, or watts) and in time (s).
8 Min.	Indicates the minimum data value (in volts, amps, or watts) between the marker locations of the selected waveform. Also indicates the distance in time of the minimum value in relation to the present trigger position.
9 Avg.	Calculates the average data value (in volts, amps, or watts) between the marker locations of the selected waveform. Time indicates the time between markers over which the average value is calculated. *For all the measurements in rest of this work, we only consider the average values of power consumption and elapsed time for the power trace in between the m1 and m2 markers that are indicated by the current 'Avg.' field.*
10 Max.	Indicates the maximum data value (in volts, amps, or watts) between the marker locations of the selected waveform. Also indicates the distance in time of the maximum value in relation to the present trigger position.

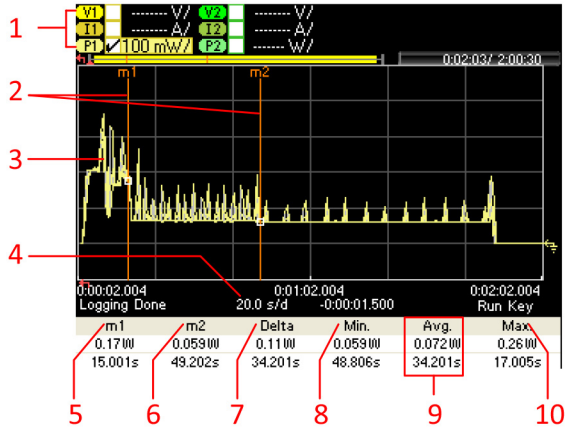

Fig. 3. Measurement Setup with Keysight N6705C DC Power Analyzer: Example of an NB-IoT waveform and measurement information available in the marker view.

real network with on-field measurements from the PA. For all the power measurements and energy calculations for rest of the waveforms/traces in this article, Label 9 provides an average power consumption and average timings between the m1 and m2 markers. These markers are set to various positions on the respective power traces of the BG96 radio transceiver, so as to obtain the adequate power consumption and timings details for the various states of its RRC operation.

C. Empirical Results

A number of experiments were conducted using two CoTS NB-IoT radio modules operating under two MNOs operating NB-IoT test networks in Tallinn, Estonia. To verify and evaluate the correctness of our proposed model, various timings for the different states of the NB-IoT radio modules were tried and tested for different power saving schemes. The generated results were tested for various versions of the FWs of these radio modules to verify their impact on the performance of the NB-IoT radio as they are continuously updated and to see to what extent they are compliant with the 3GPP defined NB-IoT standards. Our obtained results from these tests are explained in the subsections that follow.

1) Testing Active Waiting (C-DRX) Mode of the Avnet BG96 Radio Under Operator1 Network: To evaluate the detailed energy consumption of the C-DRX mode of the BG96 radio, we set the network parameters as C-DRX = 1, eDRX = 0, and PSM = 0 and obtained our empirical results for Operator1 network, as shown in Fig. 4. It could be observed that Operator1 had no limitations on the duration of its C-DRX mode as the radio remains in its active waiting state for as long as it was powered on. This is shown in Fig. 4(b), where the average power consumption for the entire C-DRX mode is measured to be 0.082 W. Fig. 4(c) details that each C-DRX cycle of 2.56 s with an average power consumption of 0.082 W. Fig. 4(a) details the attach procedure of the BG96 radio with the Operator1 network with an average power consumption of 0.18 W over 18.6 s.

During the second phase of the same experiment, the C-DRX mode of the BG96 radio was limited to a duration of 1 m, after which the radio was forced to switch to its PSM state, as shown in Fig. 5. The respective average power consumption for the C-DRX mode and C-DRX cycle, as shown in Fig. 5(a) and (c), was found to be the same as previously. However, the average power consumption of the PSM of the BG96 radio was found to be 0.19 mW, as shown in Fig. 5(b).

2) Testing Idle Waiting (eDRX) Mode of Avnet BG96 Radio Under Operator1 Network: To evaluate the fine-grained energy consumption of the eDRX mode of the BG96 radio with the underneath details of its eDRX cycle(s) that includes an eDRX_Opportunity and a PTW, and the underneath I-DRX cycles of each PTW, we carried out a second series of experiments, where we set the network parameters as C-DRX = 0, eDRX = 1, and PSM = 1 with T3324 timer = 4 m; such that the eDRX mode runs for 4 min and then switches to its PSM state. Our results from these experiments are summarized in Fig. 6. The average power consumption for the entire eDRX mode was found to be 0.071 W, as shown in Fig. 6(a), 0.070 W

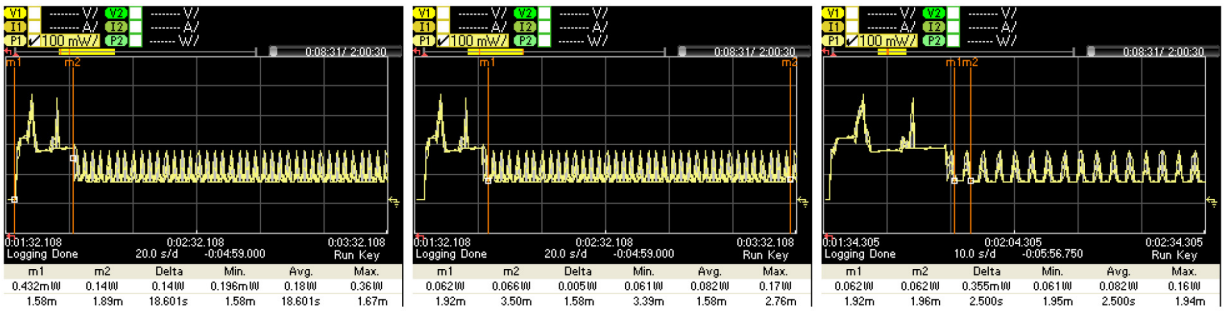

(a) (b) (c)

Fig. 4. Continuous CDRX Mode with BG96/Avnet shield under Operator 1. (a) Power trace of UE's Attach procedure with an average power consumption of 0.18 W. (b) Power trace of C-DRX mode with an average power consumption of 0.082 W. (c) Power trace of UE's C-DRX cycle with an average power consumption of 0.082 W.

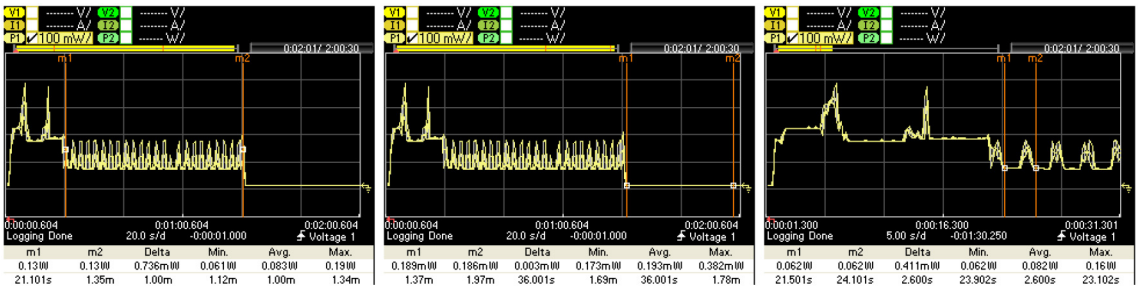

(a) (b) (c)

Fig. 5. Controlled C-DRX Mode with BG96/Avnet shield under Operator1. (a) Power trace of UE's C-DRX mode with an average power consumption of 0.083 W. (b) Power trace of UE's PSM with an average power consumption of 0.19 mW. (c) Power trace of UE's C-DRX cycle with an average power consumption of 0.082 W.

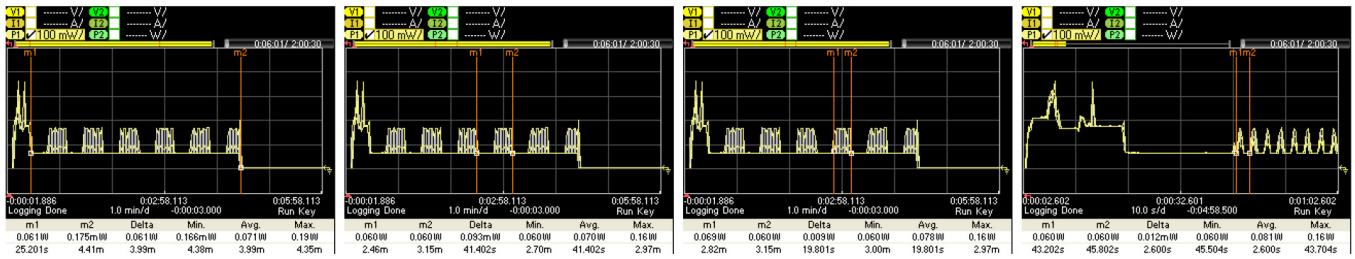

(a) (b) (c) (d)

Fig. 6. eDRX Mode (i.e., C-DRX = 0, PSM = 1, and T3324 = 4 m) with BG96/Avnet shield under Operator1. (a) Power trace of UE's eDRX mode with an average power consumption of 0.071 W. (b) Power trace of UE's eDRX cycle with an overall average power consumption of 0.070 W. (c) Power trace of UE's PTW with an average power consumption of 0.078 W. (d) Power trace of I-eDRX cycle with an average power consumption of 0.081 W.

for each eDRX cycle of 41.40 s, as shown in Fig. 6(b), and 0.078 W for the PTW of 19.80 s each, as shown in Fig. 6(c). The I-DRX cycle was found to be 2.56 s with an average power consumption of 0.081 W, as shown in Fig. 6(d).

3) Testing Power Cycle (a Repeated Sequence of C-DRX, eDRX, and PSM) of the Avnet BG96 Radio Under Operator1 Network: In these set of experiments, we evaluated the fine-grained energy consumption of the BG96 radio in a power cycle consisting of the C-DRX mode, eDRX-Mode, and PSM with the T3324 timer set to 4 min and T3412 timer set to 1 h; the results are shown in Fig. 7. All the obtained results were found to be the same as in the previous Experiment 1 and Experiment 2. Furthermore, it was observed that the radio automatically woke up from its PSM to reattach with the network and repeat its power cycle with its previous settings. The power traces for the C-DRX, eDRX, and PSM states during these experiments are shown in Fig. 7(a)–(c), respectively.

Furthermore, we transmitted 10 bytes of data from the BG96 radio on Operator1 network using UDP protocol at different CEL, as shown in Fig. 8(a) and (b). It was observed that the radio consumed 0.000372 Wh to transmit data at CEL = 0; whereas, it consumed 0.000816 Wh to transmit the same data at CEL = 1, i.e., an increase of 124.09%.

4) Testing Power Cycle of the Avnet BG96 Radio Under Operator2 Network: All the above experiments were repeated with the Avnet BG96 shield under similar conditions but this time with Operator 2's network. The obtained results from these tests are summarized in Fig. 9. During these tests, it was observed that Operator 2's network had more restrictions on

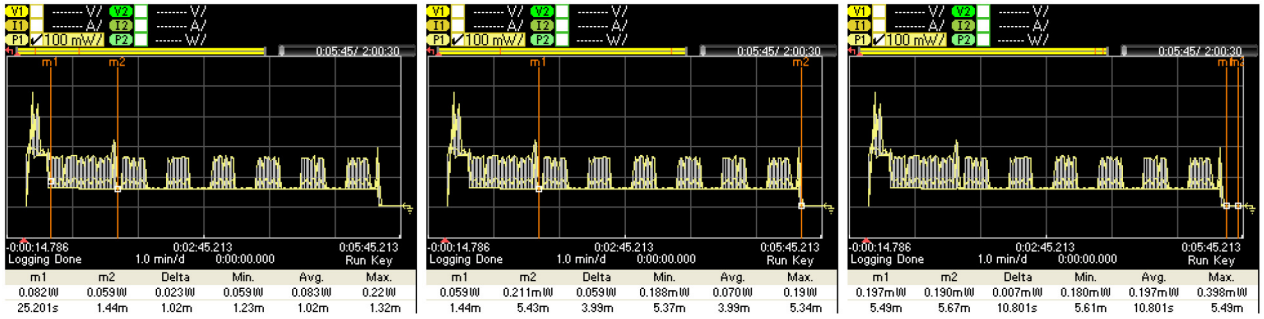

(a) (b) (c)

Fig. 7. Power cycle with BG96/Avnet shield under Operator1 network. (a) C-DRX mode runs for 1.0 min (UE configured). (b) eDRX mode runs for 4 min (UE-configured). (c) PSM runs for 60 min (UE-configured), not shown in full for readability.

TABLE IV
SUMMARY OF THE POWER CONSUMPTION OF VARIOUS STATES OF THE AVNET SILICA BG96 SHIELD UNDER THE OPERATOR1 NETWORK

Avnet Silica BG96 shield current and power consumption details with a constant 3.3V power supply		
Operational Modes	***Avg Current***	***Avg Power***
Attach/Resume Procedure (≈ 18s)	**56.8 mA**	**180 mW**
C-DRX Mode(Not fixed to any value)	**25.1 mA**	**82 mW**
C-DRX Cycle = 2.56 s	25.1 mA	82 mW
On duration (PO) = 1.28 s	32 mA	110 mW
Off duration (SP) = 1.28 s	18.1 mA	59 mW
eDRX Mode (as defined by T3324 = 4 m)	**21.8 mA**	**71 mW**
eDRX Cycle= 40.96 s	21.8 mA	70 mW
PTW = 20.48 s	25.5 mA	78 mW
I-eDRX Cycle = 2.56 s	24.47 mA	81 mW
On duration (PO) = 1.28 s	31 mA	110 mW
Off duration (SP) = 1.28 s	17.98 mA	59 mW
eDRX Opportunity = 20.48 s	17.97 mA	59 mW
PSM Mode (as defined by (T3412-T3324) value)	**0.05 mA**	**0.19 mW**

their network parameters as compared to Operator 1, i.e., the UE/radio had little provisions to configure the network parameters. For example, the C-DRX mode was fixed to 34 s (during all our tests); whereas, the eDRX mode and PSM could be configured by the UE as desired. However, the eDRX cycle and its underneath PTW in the C-DRX mode could not be configured (contrary to the case with Operator 1). It was also noted that the radio took 12.6 s on average to get connected to Operator 2's network, as compared to an average of 18 s on Operator 1's network.

Furthermore, we transmitted 10 bytes of data from the BG96 radio on Operator 2's network using the UDP protocol at different CEL, as shown in Fig. 10(a) and (b). It was observed that the radio consumed 0.00011 Wh at CEL = 0; whereas, it consumed 0.00016 Wh to transmit the same data at CEL = 1, i.e., an increase of 45.45%. Similarly, a comparison between the effects of overheads involved in the two data transmission protocols (i.e., UDP and HTTPs) on the energy consumption of the radio was also made, where the desired data of 10 bytes (that were required to be sent from the radio) were transmitted from the BG96 radio on Operator 2's network at different CEL, with additional 61 bytes of data that were the requirement of the HTTPs protocol for its server setup. The obtained power traces from these experiments are shown in Fig. 11(a) and (b). It was observed that the radio consumed 0.00052 Wh at CEL = 0 and 0.00080 Wh at CEL = 1 for the transmission of the same 71 Bytes of data through the HTTPS protocol, i.e., an increase of 53.8% in the energy

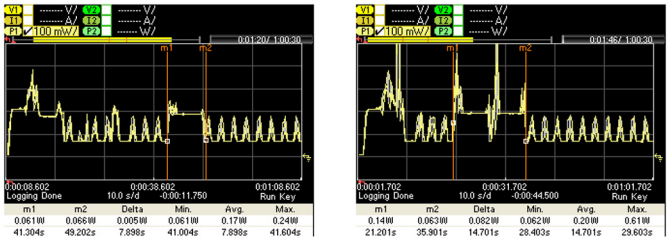

(a) (b)

Fig. 8. Transmitting ten bytes of data using UDP protocol on Operator1 network. (a) Data Transmission at CEL = 0 consumes 0.17 W for 7.898 s (0.000372 Wh). (b) Data Transmission at CEL = 1 consumes 0.20 W for 14.701 s (0.000816 Wh), i.e., an increase of 119.35%.

consumption when the CEL changed, i.e., the radio transmits for longer time because of the lower signal strength. In comparison to the UDP transmission protocol, this was an increase of 372% and 400% at CEL = 0 and CEL = 1, respectively, because of transmitting the extra 61 bytes of data overhead.

Tables IV and V summarize the power consumption of various states of the Avnet Silica BG96 shield under Operator1 and Operator2 test networks, respectively.

5) Verifying Our Results for Operator1 and Operator2 Networks With Quectel BG96 EVB Kit: All the above experiments were repeated for both the operators on the same location and under similar conditions using the Quectel BG96 EVB kit [30]. Since similar power graphs for C-DRX, eDRX,

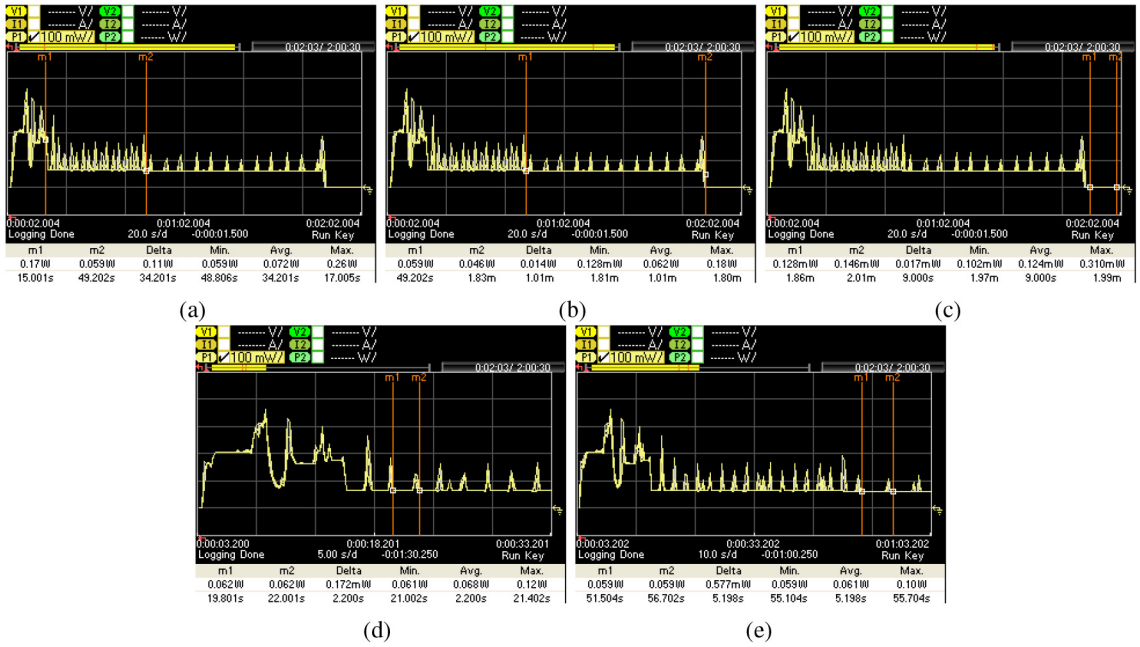

Fig. 9. Power cycle of the Avnet BG96 shield under Operator2 network: (a) C-DRX mode runs for 34.2 s, (b) eDRX mode runs for 1.0 min (UE configured), and (c) PSM runs for 1.0 h (UE configured), not shown in full for readability. In the Operator 2 network, the C-DRX Cycle is 2.1 s while the I-DRX Cycle is 5.12 s.

TABLE V
SUMMARY OF THE POWER CONSUMPTION OF VARIOUS STATES OF THE AVNET SILICA BG96 SHIELD UNDER THE OPERATOR2 NETWORK

Avnet Silica BG96 shield current and power consumption details with a constant 3.3V power supply		
Operational Modes	***Avg Current***	***Avg Power***
Attach/Resume Procedure (≈ 12 s)	**40.1 mA**	**190 mW**
C-DRX Mode (Fixed to 34 s)	**21.3 mA**	**72 mW**
C-DRX Cycle = 2.1 s	21.2 mA	70 mW
On duration (PO) = 0.5 s	28 mA	98 mW
Off duration (SP) = 1.6 s	18.6 mA	62 mW
eDRX Mode (as defined by T3324)	**19.2 mA**	**63 mW**
eDRX Cycle = 5.12 s (Fixed)	18.8 mA	62 mW
On duration (PO) = 0.3 s	26.2 mA	87 mW
Off duration (SP) = 4.7 s	18.2 mA	60 mW
PSM Mode (as defined by (T3412-T3324) value)	**0.03 mA**	**0.12 mW**

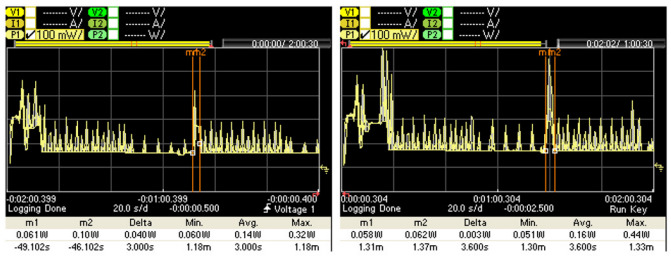

Fig. 10. Transmitting ten byte of data using UDP protocol on Operator2 network. (a) Data Transmission at CEL = 0 consumes 0.14 W for 3 s (0.00011 Wh). (b) Data Transmission at CEL = 1 consumes 0.16 W for 3.6 s (0.00016 Wh), i.e., an increase of 45.45%.

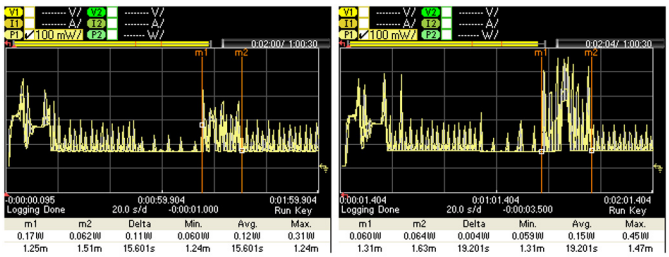

Fig. 11. Transmitting 71 bytes of data to ThingSpeak server [35] using HTTPS protocol on Operator2 network. (a) Data Transmission at CEL = 0 consumes 0.12 W for 15.6 s (0.00052 Wh). (b) Data Transmission at CEL = 1 consumes 0.15 W for 19.2 s (0.0008 Wh), i.e., an increase of 53.84%.

and PSM modes of the BG96 radio were obtained from the PA, these graphs are not included in this article for conciseness. Nevertheless, the results obtained for all these tests are summarized in Tables VI and VII, respectively.

Finally, a side-by-side comparison of the current and power consumption of the two boards, i.e., Avnet BG96 shield and Quectel BG96 EVB kit, for both the networks, i.e., Operator 1 and Operator 2, are summarized in Tables VIII and IX.

D. Summary and Discussion of the Measurement Results

In the remainder of this section, we summarize our main observations of the experimental results and present a discussion thereof.

TABLE VI
SUMMARY OF THE POWER CONSUMPTION OF VARIOUS STATES OF QUECTEL BG96 EVB KIT UNDER THE OPERATOR1 NETWORK

QUECTEL BG96 Kit current and power consumption details with a constant 3.8V power supply		
Operational Modes	***Avg Current***	***Avg Power***
Attach/Resume Procedure (≈ 18 s)	**51.8 mA**	**200 mW**
C-DRX Mode(Not fixed by the operator)	**26.1 mA**	**100 mW**
C-DRX Cycle = 2.56 s	25.6 mA	97 mW
On duration (PO) = 1.28 s	30.6 mA	120 mW
Off duration (SP) = 1.28 s	20.1 mA	78 mW
eDRX Mode (as defined by T3324 = 4 m)	**20.22 mA**	**77 mW**
eDRX Cycle= 40.96 s	20.22 mA	77 mW
PTW = 20.48 s	22.77 mA	87 mW
I-eDRX Cycle = 2.56 s	22.57 mA	86 mW
On duration (PO) = 1.28 s	27.6 mA	100 mW
Off duration (SP) = 1.28 s	16.9 mA	66 mW
eDRX Opportunity = 20.48 s	17.1 mA	66 mW
PSM Mode (value of (T3412-T3324))	**0.05 mA**	**0.20 mW**

TABLE VII
SUMMARY OF THE POWER CONSUMPTION OF VARIOUS STATES OF QUECTEL BG96 EVB KIT UNDER THE OPERATOR2 NETWORK

QUECTEL BG96 kit current and power consumption details with a constant 3.8V power supply		
Operational Modes	***Avg Current***	***Avg Power***
Attach/Resume Procedure (≈ 12s)	**59.3 mA**	**190 mW**
C-DRX Mode (Fixed to 34 s)	**25.3 mA**	**86 mW**
C-DRX Cycle = 2.1 s	25.2 mA	85 mW
On duration (PO) = 0.5 s	28 mA	170 mW
Off duration (SP) = 1.6 s	18.6 mA	78 mW
eDRX Mode (as defined by T3324)	**19.2 mA**	**63 mW**
eDRX Cycle = 5.12 s (Fixed)	30.8 mA	100 mW
On duration (PO) = 0.4 s	29.8 mA	98 mW
Off duration (SP) = 4.7 s	22.9 mA	76 mW
PSM Mode (value of (T3412-T3324))	**0.05 mA**	**0.19 mW**

TABLE VIII
SIDE BY SIDE COMPARISON OF THE AVERAGE POWER MEASUREMENTS OF AVNET BG96 SHIELD AND QUECTEL BG96 EVB KIT UNDER OPERATOR1 AND OPERATOR2 NETWORKS

Power Consumption of the Avnet BG96 shield and Quectel BG96 EVB Kit				
Avnet \ Quectel	**Attach (mW)**	**CDRX (mW)**	**eDRX (mW)**	**PSM (mW)**
Operator 1	200 / 180.0	100 / 82.0	77.0 / 71.0	0.20 / 0.19
Operator 2	190 / 190.0	86.0 / 72.0	63.0 / 63.0	0.19 / 0.12

TABLE IX
SIDE BY SIDE COMPARISON OF THE AVERAGE CURRENT MEASUREMENTS OF AVNET BG96 SHIELD AND QUECTEL BG96 EVB KIT UNDER OPERATOR1 AND OPERATOR2 NETWORKS

Current consumption of the Avnet BG96 shield and Quectel BG96 EVB Kit				
Avnet \ Quectel	**Attach (mA)**	**CDRX (mA)**	**eDRX (mA)**	**PSM (mA)**
Operator 1	51.8 / 56.8	26.1 / 25.1	20.22 / 21.8	0.05 / 0.05
Operator 2	59.3 / 40.1	25.3 / 21.3	19.2 / 19.2	0.05 / 0.03

For the results shown in Tables IV–IX, the experiments were repeated in the order of 100 times and the values were averaged accordingly. As indicated previously, Table IV summarizes the current and power consumption details of the Avnet shield under Operator1's network; whereas, Table V summarizes the current and power consumption details of the Avnet board under Operator2's network. Comparing the current and power data from both of these tables, it can be noted that with Operator1's network, the BG96 radio consumes more power on average for most of its operational modes as compared to when operating under Operator2' network. It can also be noted that contrary to the other radio modes, the power and current data values for the PSM are the same with both networks.[1]

The same observations stand true when comparing the current and power consumption data in Tables VI and VII

[1]It is also noted that the average current consumption for PSM = 0.05 mA, which is higher than the 0.01 mA value indicated in the datasheet [31]. Such a difference can be due to the additional components needed to implement a BG96 minimum system on the Avnet shield (e.g., power regulator, USB interface, etc.). Such a difference is also in line with our observation that, in a practical system, the energy consumption of NB-IoT radio transceivers is often under-estimated.

obtained for the Quectel BG96 EVB kit for both of these networks. It is clear that the BG96 radio consumes more power on average for most of its operational modes when connected to Operator1's network as compared to Operator2.

However, comparing the current and power consumption data as obtained for both of these boards , i.e., Avnet Silica and Quectel EVB kit, it is also clear that the latter consumes more for the same network parameters and under the same network conditions.

To have a better overview of all the data from the above-mentioned tables, we have further summarized them in Tables VIII and IX. All in all, it can be said that from the network side Operator1 has a higher energy consumption, while from the device side, the Quectel EVB Kit consumes more than the AVNET shield.

While the current and power consumption differences between the two boards can be explained by the fact the Quectel EVB kit features more active components than the Avnet Silica board, the differences between the two networks call for a more detailed discussion, as presented in what follows.

An essential point to keep in mind is that the UE settings affect its energy consumption to a great extent, in particular in terms of active waiting, idle waiting and PSM. At the same time, these also have a notable impact on the application QoS. In parallel, the network settings also have a significant impact on the energy consumption of the UE. In more details:

1) the inactivity timer is operator specific; thus, depending on the network configuration, this can be a major energy-saving factor on the UE side. Our results have shown that Operator2 provides greater flexibility in terms of control and configurability of the C-DRX (within the inactivity timer) mode as compared to Operator1. On the other hand, Operator1 does not limit the length of its active waiting period (within the inactivity timer). This explains why Operator1 consumes more as compared to Operator 2 since the latter has a controlled active waiting period. Moreover, since the inactivity timer is reset after each downlink data exchange, the longer its span the larger its impact on the UE energy consumption. Similarly, if downlink data are received in fragments, the energy consumption due to the inactivity timer will add up;
2) the activity timer is UE configurable, but its underneath eDRX cycles with its PTW and its underneath I-DRX cycles are network specific; thus, their settings affect the overall energy consumption of the UE. Operator2 also provides a greater flexibility in terms of control and configurability of its eDRX settings as compared to Operator1; since the former supports more robust settings for these parameters, it is thus more energy friendly from the UE perspective. However, the effects of such parameters on the QoS of application are still unknown and beyond the scope of this article. Though Operator 1 provides more flexibility in these settings, the overall energy consumption of the radio is higher;
3) the power consumption of the PSM of the radio is nearly identical with both operators. This can be explained by the fact that when in the PSM mode, most parts of the radio module are turned off and no operator-specific parameter affects the current drawn by the chip. However, a general comment is that while the longer the radio stays in PSM, the larger its energy savings, this translates in increased latency cost and, thus, possibly reduced QoS for the application. This important tradeoff in NB-IoT is not yet fully explored in the literature;
4) our experiments have also shown that the transmission power varies with the signal strength of the radio and, thus, affects the UE energy consumption. The transmit power can be ramped-up to a maximum of 23 dBm, whether when connecting to the BS or while transmitting data. For example, in Fig. 11(a), it can be seen that the power for data transmission is 0.12 W (i.e., 20.79 dBm) and 0.15 W (i.e., 21.76 dBm) in Fig. 11(b). Since the UE has no provision to control its transmit power, the energy consumption from the UE transmit power point of view is not an exclusive UE feature;
5) the data transmission protocol varies in terms of their control overheads, data payloads, CEL, and security/guarantees. These various aspects yield different energy consumption as seen in our experimental results when transmitting data with the UDP and HTTPs protocols in two different coverage classes. For example, Figs. 8 and 10 show that transiting from the CEL $= 0$ to CEL $= 1$ with UDP leads to energy consumption increases between 45% and 119%, i.e., up to more than a factor 2. Fig. 11(a) and (b) shows that the same transition with HTTPs leads to an increase of 53.84%, i.e., slightly more than a factor 1.5. Also, as mentioned earlier, the increase between UDS and HTTPs ranges from 372% and 400%.

Moreover, from the results obtained through these experiments, it is clear that almost all of the 3GPP defined UE states are attainable on both MNO's test networks, and thus by extension on commercial networks; this is in stark contrast to what has been reported in most of the existing literature so far. The results also indicates that all the power saving features of the NB-IoT technology are included in the considered CoTS NB-IoT radio chips and could be utilized as per the application requirements. However, as the hardware and software developments of NB-IoT are ongoing, special care must be taken to choose the right firmware for the right hardware that is being used for the specific application. Our results also show that all the timers are flexible and can be set as per the 3GPP standards provided the network operators allow any such provisions from the network side and this should be kept in mind by application developers to obtain network access.

V. Evaluation of Our Proposed Model

Section IV has presented individual empirical measurement results for various timings for the different states of the NB-IoT radio module for different power saving schemes. Next, in this section we: 1) evaluate the error of our proposed model by calculating the difference between the energy consumption obtained from the real-life deployment versus that predicted by

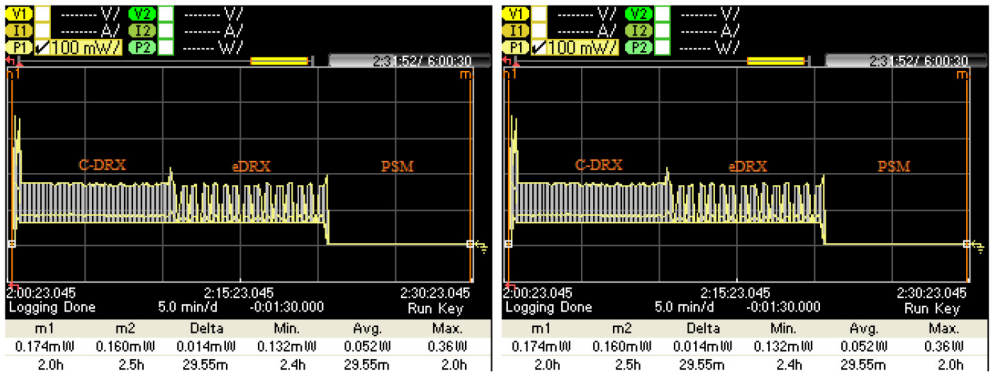

Fig. 12. Power traces of the first evaluation test with the Avnet BG96 shield operating on Operator1 network. (a) Power cycle of 30 min ("29.55 m" displayed between m1 and m2 markers) that includes an Attach procedure of 18 s, C-DRX, e-DRX, and PSM of a bit less than 10 min each. (b) Power cycle of (a) is repeated two times in an observation window of 60 min ("59.53 m" displayed between m1 and m2 markers).

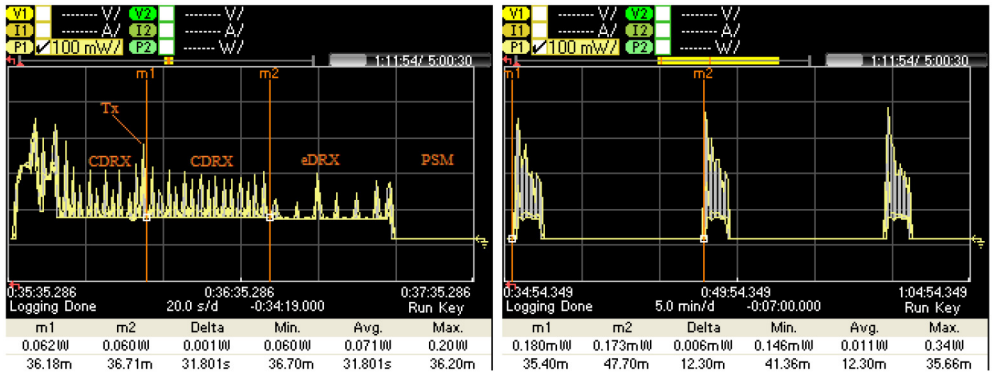

Fig. 13. Power traces of the second evaluation test with Avnet BG96 shield on Operator2 network. (a) Power cycle of 12.3 min that includes an Attach procedure of 12.1 s, C-DRX mode of 20 s, Tx (10 bytes data over UDP) of 3 s, repeated C-DRX of 32 s ("31.801 s" displayed between m1 and m2 markers), eDRX of 34 s and PSM of a bit more than 10 min (not shown in full for readability). (b) Power cycle of (a) 12.3 min ("12.30 m" displayed between m1 and m2 markers) is repeated 3 times (the last PSM phase is not shown in full for readability).

the model and 2) we summarize the sensitivity analysis conducted to evaluate which parameters have the largest impact on the total energy consumption in our proposed model.

A. Model Evaluation Tests

We have conducted three sets of experiments of which the base cycle lasts from 12.3 min to 1.2 h and is repeated from 2 to 10 times during the observation window. Doing so forces the NB-IoT radio in various operational conditions and allows characterizing the average differences between the energy consumption predicted by the model and the real-life values. The three sets of experiments use the Avnet BG96 shield operating on the Operator1 or Operator2 network, as described in what follows.

The first evaluation test was executed with an Avnet BG96 shield board operating on the Operator1 network. The test consisted of a base power cycle of 30 min as captured between m1 and m2 (29.55 min shown) in Fig. 12(a) and repeated twice in an observation window of 1 h (59.53 min shown) between m1 and m2, as shown in Fig. 12(b). As can be seen in Fig. 12(a), the base power cycle includes an attach procedure of 18 s, and C-DRX, e-DRX, and PSM states of a bit less than 10 min each where the average power consumption for the base power cycle is 0.052 W. As can be seen in Fig. 12(b), it is repeated twice over a period of 60 min captured between m1 and m2 (59.53 min shown), where the average power consumption is found to be 0.052 W. The energy consumed per each power cycle as per (19) is 0.022 Wh; whereas, that measured with the PA is 0.026 Wh. The energy consumed for the entire observation window as per (19) is 0.044 Wh; whereas, that measured with the PA is 0.052 Wh, i.e., an error of 15.38%, as indicated in Table X.

The second evaluation test was also conducted with an Avnet BG96 shield, but this time operating on Operator2 network. The test consisted of the base power cycle shown in Fig. 13(a) (m1 and m2 in this figure are used to record the repeated C-DRX cycle of the radio after a data transmission (Tx)); this power cycle is repeated three times as shown in Fig. 13(b). The base power cycle lasts 12.3 min and includes an Attach procedure of 12.1 s, C-DRX mode of 20 s, Tx through UDP protocol of 3 s, repeated C-DRX of 32 s, eDRX of 34 s, and PSM of a bit more than 10 m. The base power cycle consumes on average 0.011 W during the 12.3-min duration, i.e., an average energy consumption of 0.0022 Wh. As indicated in Table X, the energy consumed per power cycle as per (19) is 0.0024 Wh, i.e., an error of 9.09%.

TABLE X
NB-IoT RADIO ENERGY CONSUMPTION ERROR: PROPOSED MODEL VERSUS REAL-LIFE EVALUATION TESTS

Test setup	Energy as per model (Wh)	Energy as per measurement (Wh)	Relative Error (%)
Avnet BG96 shield, Operator1	0.052	0.044	15.38
Avnet BG96 shield, Operator2	0.0024	0.0022	9.09
Avnet BG96 shield, Operator2	0.01204	0.01200	0.33

(a) (b)

Fig. 14. Power traces of the third evaluation test with Avnet BG96 shield under Operator2 network. (a) Power cycle of 1.2 h ("1.2 h" between m1 and m2 markers) including an Attach procedure of 12.1 s, C-DRX of 32 s, e-DRX of 10 min, and PSM of 64 min. (b) Power cycle of (a) is repeated ten times in an observation window of 11.8 h ("11.8 h" between m1 and m2 markers). (Note that some of the PSM durations are shorter than others).

Like the second one, the third evaluation test was conducted with the Avnet BG96 shield operating under the Operator2 network, but this time for a longer duration. The base cycle lasts 1.2 h, including an Attach procedure of 12 s, CDRX of 32 s, e-DRX of 10 min, and PSM of 64 min, as shown in Fig. 14(a). This power cycle of 1.2 h has an average power consumption of 0.010 W. It is then repeated ten times in an observation window of 11.8 h, as shown in Fig. 14(b) (note that some of the PSM durations are shorter than others). In this case, the energy consumed per power cycle measured with the PA is 0.01200 Wh; whereas, as per (19), it is found to be 0.01204 Wh, i.e., an error of 0.33% only, as indicated in Table X.

The error of the proposed model ranges from as low as 0.33% for longer durations (e.g., when the radio has to activate after several hours or more), and reaches up to approximately 15.38% for shorter durations (e.g., when the radio has to activate after several minutes to hours). Since the majority of NB-IoT applications are intended for longer duration scenarios, the error will lie on the smaller end; as also indicated by the sensitivity analysis of the model.

Regarding system noise and environmental noise, we have used CoTS NB-IoT devices in order to create a realistic energy consumption model that reflects the practical performance of such devices, including possible inherent system noises. Furthermore, precautions (grounding of measurement equipment, etc.) were taken when carrying out our experiments, and no environmental noises were observed during our measurement campaign. Regarding interference, although there could be an impact due to intercell and intracell interferences, we have not experienced such interferences due to the limited number of devices connected to our test networks (the issue of intercell interference has been investigated in our previous work [36], [37], i.e., 10%–15% throughput can be improved while exploiting inference minimization schemes).

TABLE XI
SENSITIVITY ANALYSIS OF THE POWER CONSUMPTION PARAMETERS OF BG96 RADIO

BG96 Power Parameters						
P_{TAU}	P_{ATTACH}	P_{TX}	P_{RX}	P_{CDRX}	P_{eDRX}	P_{PSM}
0.18W	0.18W	0.17W	0.16W	0.083W	0.070W	0.0002W

B. Summary of the Sensitivity Analysis of the Model

The sensitivity analysis (SA) was carried out on both the power consumption parameters and timings parameters of the proposed model.

The SA of the power consumption parameters, i.e., P_{ATTACH}, P_{TX}, P_{RX}, P_{CDRX}, P_{eDRX}, P_{PSM}, and P_{TAU}, of our proposed model indicates that they are technology-dependent and may vary for various chipsets. For example, typical values for the power consumption parameters of the BC95 chipset (an advanced IoT chipset from Quectel) are slightly lower than those for the BG96 chipset from the same vendor. Similarly, the values for these power parameters may also differ slightly from vendor to vendor. That is why these power parameters affect the overall energy consumption of the radio but only to a smaller extent. Since we have used BG96 chipset-based modules for all our experiments in this work, we thus decided to use the values for the power consumption parameters of BG96 chipset; with a possible impact on the overall energy consumption of the radio in a descending order as shown in Table XI.

On the other hand, the timing parameters of the proposed model, i.e., T_{ATTACH}, T_{TX},T_{RX}, T_{CDRX}, T_{eDRX}, T_{PSM}, and T_{TAU} have their minimum and maximum values (as standardized by 3GPP) as given in Table XII.

The sensitivity analysis of these timing parameters indicates that they have an impact on the total energy consumption of the radio, in a descending order, as explained as follows.

TABLE XII
SENSITIVITY ANALYSIS OF THE TIMINGS PARAMETERS OF NB-IOT RADIO

Minimum and Maximum values for the Timing Parameters				
T_{TAU} / T_{ATTACH}	T_{TX} / T_{RX}	T_{CDRX}	T_{eDRX}	T_{PSM}
18.6s - # of attempts	0s–# of transmissions	10s–60s	0s–186m	0s–413d

1) T_{ATTACH} has the most impact on the overall energy consumption of the radio, especially when the radio wakes up frequently (e.g., in patterns of a few minutes). However, in less frequent scenarios (e.g., once per day or weeks), its impact is negligible. Furthermore, the TAU procedure has almost the same effect as that of the ATTACH procedure (especially from the practical perspective).
2) The active waiting period, i.e., T_{CDRX} and the idle waiting period, i.e., T_{eDRX} have almost an equal impact on the total energy consumption of the radio. However, since the Inactivity timer is limited by the operator (usually set to lower than 60 s), its impact on the total energy consumption is lower as compared to T_{CDRX} of relatively longer durations.
3) Similarly, the impact of the payload size both in (T_{TX}, T_{RX}) is not significant on the total energy consumption of the radio while the radio is operating in good coverage. However, as the coverage worsens, its impact adds up as a function of the number of repetitions that an NB-IoT radio has to perform in that CEL.
4) Finally, the effect of PSM and its benefits in terms of the total energy consumption of the radio becomes substantial only when enabled for longer durations.

VI. CONCLUSION

NB-IoT is an emerging technology, which is expected to dominate the IoT landscape in terms of wireless communication technology for massive machine-type communication. Understanding the energy budget of NB-IoT is important; however, this is weakly addressed in the state of the art. The motivation of this work was thus to provide a modeling methodology for profiling the baseline energy consumption of an NB-IoT radio transceiver based on the RRC protocol standardized by 3GPP. The proposed energy consumption model provides a detailed and realistic NB-IoT radio transceiver energy consumption model; the detailed analysis of the RRC protocol and empirical measurements illustrates the fine-grained energy consumption of the RRC protocol for two development boards operating on two MNOs test networks. Finally, the real-life empirical evaluation results showed that the error of the proposed model ranges between 0.33% and 15.38%. The proposed model and its evaluation ensure that it is viable to be used as a reference benchmark for NB-IoT radio communication. In the future, we will explore energy consumption optimization strategies depending on the lifetime requirement of a given application; the proposed baseline energy consumption model will be used to evaluate the impact of such optimization strategies.

REFERENCES

[1] A. Rico-Alvarino *et al.*, "An overview of 3GPP enhancements on machine to machine communications," *IEEE Commun. Mag.*, vol. 54, no. 6, pp. 14–21, Jun. 2016.
[2] Y.-P. E. Wang *et al.*, "A primer on 3GPP narrowband Internet of Things," *IEEE Commun. Mag.*, vol. 55, no. 3, pp. 117–123, Mar. 2017.
[3] P. Mekikis *et al.*, "NFV-enabled experimental platform for 5G tactile Internet support in industrial environments," *IEEE Trans. Ind. Informat.*, vol. 16, no. 3, pp. 1895–1903, Mar. 2020.
[4] J. Serra, L. Sanabria-Russo, D. Pubill, and C. Verikoukis, "Scalable and flexible IoT data analytics: When machine learning meets SDN and virtualization," in *Proc. IEEE 23rd Int. Workshop Comput. Aided Model. Design Commun. Links Netw. (CAMAD)*, 2018, pp. 1–6.
[5] *Medium Access Control (MAC) Protocol Specification (Release 8), Version 8.0.0*, 3GPP Standard TS 36.321, 2008.
[6] *Evolved Universal Terrestrial Radio Access (E-UTRA); Radio Resource Control (RRC); Protocol Specification (Release 10)*, 3GPP Standard TS 36.331, 2012.
[7] *Radio Resource Control (RRC)*, 3GPP Standard TS 36.331, 2012.
[8] C.-W. Chang and J.-C. Chen, "Adjustable extended discontinuous reception cycle for idle-state users in LTE-A," *IEEE Commun. Lett.*, vol. 20, no. 11, pp. 2288–2291, Nov. 2016.
[9] A. K. Sultania, C. Delgado, and J. Famaey, "Implementation of NB-IoT power saving schemes in ns-3," in *Proc. Workshop Next-Gener. Wireless NS-3*, 2019, pp. 5–8.
[10] A. K. Sultania, P. Zand, C. Blondia, and J. Famaey, "Energy modeling and evaluation of NB-IoT with PSM and EDRX," in *Proc. IEEE Globecom Workshops (GC Wkshps)*, 2018, pp. 1–7.
[11] G. Tsoukaneri, F. Garcia, and M. K. Marina, "Narrowband IoT device energy consumption characterization and optimizations," in *Proc. EWSN*, 2020, pp. 1–12.
[12] C. Y. Yeoh, A. B. Man, Q. M. Ashraf, and A. K. Samingan, "Experimental assessment of battery lifetime for commercial off-the-shelf NB-IoT module," in *Proc. 20th Int. Conf. Adv. Commun. Technol. (ICACT)*, 2018, pp. 223–228.
[13] P. Andres-Maldonado, P. Ameigeiras, J. Prados-Garzon, J. Navarro-Ortiz, and J. M. Lopez-Soler, "Narrowband IoT data transmission procedures for massive machine-type communications," *IEEE Netw.*, vol. 31, no. 6, pp. 8–15, Nov./Dec. 2017.
[14] P. Andres-Maldonado, M. Lauridsen, P. Ameigeiras, and J. M. Lopez-Soler, "Analytical modeling and experimental validation of NB-IoT device energy consumption," *IEEE Internet Things J.*, vol. 6, no. 3, pp. 5691–5701, Jun. 2019.
[15] P. Andres-Maldonado, P. Ameigeiras, J. Prados-Garzon, J. J. Ramos-Munoz, and J. M. Lopez-Soler, "Optimized LTE data transmission procedures for IoT: Device side energy consumption analysis," in *Proc. IEEE Int. Conf. Commun. Workshops (ICC Workshops)*, 2017, pp. 540–545.
[16] M. El Soussi, P. Zand, F. Pasveer, and G. Dolmans, "Evaluating the performance of EMTC and NB-IoT for smart city applications," in *Proc. IEEE Int. Conf. Commun. (ICC)*, 2018, pp. 1–7.
[17] R. Mozny, P. Masek, M. Stusek, K. Zeman, A. Ometov, and J. Hosek, "On the performance of narrow-band Internet of Things (NB-IoT) for delay-tolerant services," in *Proc. 42nd Int. Conf. Telecommun. Signal Process. (TSP)*, 2019, pp. 637–642.
[18] S. S. Basu, A. K. Sultania, J. Famaey, and J. Hoebeke, "Experimental performance evaluation of NB-IoT," in *Proc. Int. Conf. Wireless Mobile Comput. Netw. Commun. (WiMob)*, 2019, pp. 1–6.
[19] B. Martinez, F. Adelantado, A. Bartoli, and X. Vilajosana, "Exploring the performance boundaries of NB-IoT," *IEEE Internet Things J.*, vol. 6, no. 3, pp. 5702–5712, Jun. 2019.
[20] S. Duhovnikov, A. Baltaci, D. Gera, and D. A. Schupke, "Power consumption analysis of NB-IoT technology for low-power aircraft applications," in *Proc. IEEE 5th World Forum Internet Thin. (WF-IoT)*, 2019, pp. 719–723.
[21] M. Lauridsen, R. Krigslund, M. Rohr, and G. Madueno, "An empirical NB-IoT power consumption model for battery lifetime estimation," in *Proc. IEEE 87th Veh. Technol. Conf. (VTC Spring)*, 2018, pp. 1–5.
[22] P. Jörke, R. Falkenberg, and C. Wietfeld, "Power consumption analysis of NB-IoT and EMTC in challenging smart city environments," in *Proc. IEEE Globecom Workshops (GC Wkshps)*, 2018, pp. 1–6.
[23] K. Mikhaylov *et al.*, "Multi-RAT LPWAN in smart cities: Trial of LoRaWAN and NB-IoT integration," in *Proc. IEEE Int. Conf. Commun. (ICC)*, 2018, pp. 1–6.
[24] M. Lukic, S. Sobot, I. Mezei, D. Danilovic, and D. Vukobratovic, "In-depth real-world evaluation of NB-IoT module energy consumption," 2020. [Online]. Available: arXiv:2005.13648.

[25] *GPRS Enhancements for Evolved Universal Terrestrial Radio Access Network (E-UTRAN) Access*, 3GPP Standard TS 23.401, 2013.
[26] *GPRS Enhancments for Evolved Universal Terrestrial Radio Access Network Access, Release 14, V14.1.0*, 3GPP Standard TS 23.401, 2016.
[27] *GPRS Enhancements for Evolved Universal Terrestrial Radio Access Network Access, Release 16, V16.6.0*, 3GPP Standard TS 23.401, 2020.
[28] *LTE; General Packet Radio Service (GPRS) Enhancements for Evolved Universal Terrestrial Radio Access Network (E-UTRAN) Access, Version 14.3.0 Release 14*, ETSI Standard TS 123 401, 2017.
[29] Avnet:Silica. *Avnet: Quality Electronic Components Services*. Accessed: Apr. 29, 2021. [Online]. Available: https://www.avnet.com/wps/portal/silica/products/new-products/npi/2018/avnet-nb-iot-shield-sensor/
[30] Quectel UMTS LTE EVB Kit. *Quectel*. Accessed: Apr. 29, 2021. [Online]. Available: https://www.quectel.com/product/umts-lte-evb-kit/
[31] Quectel LPWA IoT Module. *BG96 LTE Cat M1/NB1/EGPRS Module*. Accessed: Apr. 29, 2021. [Online]. Available: https://www.quectel.com/product/lte-bg96-cat-m1-nb1-egprs/
[32] Keysight Technologies. *N6705C DC Power Analyzer*. Accessed: Apr. 19, 2021. [Online]. Available: https://www.keysight.com/en/pd-2747858-pn-N6705C/dc-power-analyzer-modular-600-w-4-slots?cc=EE&lc=eng
[33] Digilent. *Pmod-USB-to-UART-Interface*. Accessed: Apr. 19, 2021. [Online]. Available: https://store.digilentinc.com/pmod-usbuart-usb-to-uart-interface/
[34] Avnet-Silica-team. *NBIOTBG96SHIELD-HW-Schematic*. Accessed: Apr. 19, 2021. [Online]. Available: https://github.com/Avnet-Silica-team/NBIoTBG96-HW/blob/master/BAENBIOTBG96SHIELD_RSR1157C-SCHEMA.pdf/
[35] ThingSpeak Server. *ThingSpeak for IoT Projects*. Accessed: Apr. 19, 2021. [Online]. Available: https://thingspeak.com/channels/1085017/
[36] H. Malik, H. Pervaiz, M. M. Alam, Y. Le Moullec, A. Kuusik, and M. A. Imran, "Radio resource management scheme in NB-Iot systems," *IEEE Access*, vol. 6, pp. 15051–15064, 2018.
[37] H. Malik *et al.*, "Radio resource management in NB-IoT systems: Empowered by interference prediction and flexible duplexing," *IEEE Netw.*, vol. 34, no. 1, pp. 144–151, Jan./Feb. 2020.

Sikandar M. Zulqarnain Khan received the M.Sc. degree in electronics, electrical, control and instrumentation engineering from Hanyang University, Seoul, South Korea, in 2010.

He joined the COMSATs Institute of Information Technology, Islamabad, Pakistan, as a Faculty Member. In 2014, he joined the Instituto de Telecomunicaes of Aveiro, Aveiro, Portugal, as a Researcher. He joined Scuola Superiore Sant'Anna, Pisa, Italy, as a Researcher. In 2017, he joined the School of ECE, Technical University of Crete, Chania, Greece, as a Visiting Researcher. Since 2018, he has been with Thomas Johann Seebeck Department of Electronics, TalTech, Tallinn, Estonia. He has authored several conference and journal research papers. His research interests include embedded systems, control systems, wireless communications, and embedded artificial intelligence.

Muhammad Mahtab Alam (Senior Member, IEEE) received the M.Sc. degree in electrical engineering from Aalborg University, Aalborg, Denmark, in 2007, and the Ph.D. degree in signal processing and telecommunication from the INRIA Research Center, University of Rennes 1, Rennes, France, in 2013.

In 2013, he joined the Swedish College of Engineering and Technology, Wah Cantonment, Pakistan, as an Assistant Professor. He did his postdoctoral research with Qatar Mobility Innovation Center, Doha, Qatar, from 2014 to 2016. In 2016, he joined as the European Research Area Chair holder and an Associate Professor with the Thomas Johann Seebeck Department of Electronics, Tallinn University of Technology, Tallinn, Estonia, where he was elected as a Professor, in 2018. In 2019, he become the Head of Communication Systems Research Group and leading number of National and International projects. His research interests include the fields of wireless communications and connectivity, NB-IoT 5G/B5G smart networks and services, and low-power wearable networks for SmartHealth.

Yannick Le Moullec (Senior Member, IEEE) received the M.Sc. degree from the Université de Rennes I, Rennes, France, in 1999, and the Ph.D. and HDR (accreditation to supervise research) degrees from the Université de Bretagne Sud, Lorient, France, in 2003 and 2016, respectively.

From 2003 to 2013, he successively held a Postdoctoral Researcher, an Assistant Professor, and an Associate Professor positions with the Department of Electronic Systems, Aalborg University, Aalborg, Denmark. He then joined the Thomas Johann Seebeck Department of Electronics, Tallinn University of Technology, Tallinn, Estonia: Senior Researcher from 2013 to 2016 and professorship since 2017. His research interests include embedded systems, reconfigurable systems, IoT, and application thereof. He has supervised or co-supervised more than 50 M.Sc. students and 11 Ph.D. students. He has been involved in more than 20 projects, including five as PI, co-PI, or co-main applicant; one such notable project was the H2020 COEL ERA-Chair project from 2015 to 2019. He is a member of the IEEE Sustainable ICT Technical Community and the IEEE Circuits and Systems Society.

Alar Kuusik (Member, IEEE) received the Ph.D. degree in IT from the Tallinn University of Technology (TalTech), Tallinn, Estonia, in 2001; followed by Postdoctoral program with Tokyo Denki University, Tokyo, Japan.

He currently serves the position of Estonian C/COM/IT joint Chapter Chair. He also serves the position of a Senior Researcher and a Lecturer with TalTech, focusing on IoT, biomedical sensorics, and body area networking. He has been developing commercial embedded electronic devices for U.S. and European customers and involved with several international research and innovation projects related to smart environment, telecare, and m-health. He has been consulting Estonian government and hospitals in telemedicine topics. He has published over 50 peer-reviewed articles and owns several patents.

Sven Pärand received the M.Sc. degree in telecommunications and the Ph.D. degree in electronics and telecommunication from the Tallinn University of Technology, Tallinn, Estonia, in 2006 and 2018, respectively.

He has been an Engineer with Telia Estonia Ltd., Tallinn, since 2012, initially working on IMS and migration toward the Next Generation Network. Starting form 2018, he moved on to work as a 5G development manager with the aim of deploying the 5G network with Telia Estonia. He is currently the mobile services owner at the same company, responsible for the management and development of all mobile services across all of all the mobile generations.

Christos Verikoukis (Senior Member, IEEE) received the Ph.D. degree in broadband indoor wireless communications from UPC, Barcelona, Spain, in 2000.

He is currently a Fellow Researcher Research Director (R4) with the Telecommunications Technological Centre of Catalonia, Castelldefels, Spain, and an Adjunct Professor with the University of Barcelona, Barcelona. He has authored over 140 journal articles, over 200 conference articles, three books, 14 book chapters, and three patents. He has participated in more than 30 competitive research projects, while he has supervised 19 Ph.D. students and ten Postdoctoral Researchers.

Dr. Verikoukis received the Best Paper Award at the IEEE ICC 2011 2020, the IEEE GLOBECOM 2014 and 2015, the EuCNC 2016, and the EURASIP 2013 Best Paper Award of the Journal on Advances in Signal Processing. He is currently the IEEE ComSoc EMEA Director and a Member-at-Large of IEEE ComSoc GITC.